Letter

Spin waves and magnetic Hamiltonian in the low-temperature phase of $LiInCr_4O_8$

Gøran J. Nilsen [1,2,*] Rafał Wawrzyńczak [3,4] Harald O. Jeschke [5,†] Hannu Mutka [3] Takatsugu Masuda [6] Nicola Casati [7] Vladimir Pomjakushin [8] Zenji Hiroi [6] and Yoshihiko Okamoto [6]

[1] *ISIS Neutron and Muon Source, Science and Technology Facilities Council, Didcot OX11 0QX, United Kingdom*

[2] *Department of Mathematics and Physics, University of Stavanger, 4036 Stavanger, Norway*

[3] *Institut Laue-Langevin, CS 20156, 38042 Grenoble Cedex 9, France*

[4] *Max Planck Institute for Chemical Physics of Solids, 01187 Dresden, Germany*

[5] *Research Institute for Interdisciplinary Science, Okayama University, Okayama 700-8530, Japan*

[6] *Institute for Solid State Physics, University of Tokyo, Kashiwa, Chiba 277-8581, Japan*

[7] *Swiss Light Source, Paul Scherrer Institute, 5232 Villigen PSI, Switzerland*

[8] *SINQ, Paul Scherrer Institute, 5232 Villigen PSI, Switzerland*

(Received 6 March 2025; accepted 6 June 2025; published 14 July 2025)

Transition metal spinels, particularly those containing chromium 3+ ions (Cr^{3+}), display a rich variety of low-temperature magnetostructural states. Here, we present a combined neutron scattering, synchrotron x-ray diffraction, and density functional theory study of the frustrated "breathing pyrochlore" chromium spinel $LiInCr_4O_8$, where the adjacent Cr^{3+} tetrahedra alternate in magnetic interaction strength. We first establish the low-temperature tetragonal structure from the diffraction measurements. Considering the magnetic structure in light of the distortions generated by this structure, the short magnetic correlation length found in a previous study can be explained by dimensional reduction due to residual frustration. The Heisenberg Hamiltonian for the low-temperature structure is extracted using density functional theory-based energy mapping and clearly shows the partial release of frustration due to the structural transition. The first four exchanges terms dominate, and the two nearest-neighbor exchanges J and J' in the high-temperature structure both split substantially. The full magnetic excitation spectrum obtained by inelastic neutron scattering can be accurately reproduced by a linear spin-wave theory model using the density functional exchange parameters as a starting point. However, it is found that multiple parameter sets that obey the relation $(J_1 + J_4)/(J_2 + J_3) \sim 1.24$, $J_1 > J_2$, and $J_3 > J_4$ provide an equally good description of the data. This ratio, along with the low-temperature structure, suggests that it is the distortion of the small tetrahedra that drives the magnetostructural transition.

DOI: 10.1103/wjh8-qt1x

Magnetic frustration—the inability of a system to satisfy all of its internal magnetic interactions—can lead to highly degenerate disordered states at low temperature. In most materials, however, frustration is relieved by perturbing terms in the magnetic Hamiltonian, resulting in long-range magnetic order. As a result of the high degeneracy of the parent state, the phase diagrams with respect to these perturbing interactions are often rich [1–4]. In the case of the chromium spinels ACr_2O_4, where the magnetic Cr^{3+} ions (d^3, $S = 3/2$) form a highly frustrated pyrochlore lattice of corner-sharing tetrahedra, the frustration-relieving perturbation is the exceptionally strong spin-lattice coupling [5,6]. This results in a wide variety of magnetic states and phenomena at low temperature, including fractional magnetization plateaus in the ACr_2O_4 [7,8] members of the family, and large-supercell magnetostructural order in $ZnCr_2O_4$ [9,10].

The study of chromium spinels has more recently broadened to the so-called breathing pyrochlore family $AA'Cr_4X_8$ [11–21], where the ordering of the A and A' cations on the A site produce an alternation in both the tetrahedron size and magnetic interaction strength on the pyrochlore lattice. Breathing pyrochlore materials thus provide an arena to explore the interplay between bond alternation, frustration, and spin-lattice coupling. The loss of centrosymmetry in the $F\bar{4}3m$ space group adopted by most of these materials should also lead to topological excitations [22] and, in the $S = 1/2$ limit, a range of possible spin-liquid ground states [23].

The two most-studied materials in the breathing pyrochlore family are $LiInCr_4O_8$ and $LiGaCr_4O_8$ [11,16,21,24–28], which display small and large alternations in their magnetic interaction strengths, respectively. Their degree of alternation is quantified by the breathing factor J'/J, where J' and J are the exchange constants on the large and small tetrahedra, and was estimated to be ∼0.1 for $LiInCr_4O_8$ and ∼0.6 for $LiGaCr_4O_8$ [11]. Both materials furthermore exhibit two magnetostructural phase transitions at low temperature, leading to complex phase-separated low-temperature states: In the

*Contact author: goran.nilsen@stfc.ac.uk

†Contact author: jeschke@okayama-u.ac.jp

case of $LiInCr_4O_8$, the upper transition at $T_u \simeq 17$ K has been proposed to involve a reduction in structural symmetry from cubic $F\bar{4}m3$ to tetragonal $I\bar{4}m2$ [25]. The lower transition at $T_l \simeq 13$ K coincides with the appearance of broad magnetic peaks indexed by $\mathbf{k} = (10\delta)$ ($\delta \sim 0.2$) (in the cubic basis), and has been ascribed to nearly collinear two-up two-down order. This type of order has been predicted by the so-called site-phonon model, which considers all effective multispin terms generated by collective distortions of neighboring tetrahedra [29,30]. The site-phonon model also predicts a 1/2 magnetization plateau for $LiInCr_4O_8$, which has been verified experimentally [31].

In this Letter, we demonstrate that the $I\bar{4}m2$ space group previously assigned to the low-temperature structure of $LiInCr_4O_8$ is consistent with new synchrotron powder x-ray diffraction and neutron diffraction data, and we resolve the full structure. The nearly collinear magnetic order combined with the pattern of distortions in this structure suggests that it is the distortion of the small tetrahedra that drives the transition to the low-temperature state. The more accurate atomic coordinates afforded by the new diffraction data also permit us to carry out density functional theory (DFT) calculations of the magnetic exchange parameters. Both the magnetic order and the overall structure of the spectrum are correctly predicted by these calculations. The existing inelastic neutron scattering data are reanalyzed in the context of the new DFT parameters by fitting to a linear spin-wave theory model containing all four nearest-neighbor exchanges in the distorted structure. Excellent agreement is found for a set of parameters which obey the relation $(J_1 + J_3)/(J_2 + J_4) \sim 1.24$, where $J_1 > J_2$ and $J_3 > J_4$. The fact that this ratio exceeds one is also consistent with the observed distortion pattern. Our study shows that it is possible to obtain a consistent description of both the magnetic structure and excitations in the low-temperature magnetostructural ordered phase of a chromium spinel.

The ^{7}Li-enriched powder sample of $LiInCr_4O_8$ used in the present study was the same as that used in Refs. [11,25]. For high-resolution synchrotron x-ray diffraction on the MS-X04A beamline at the Swiss Light Source (PSI, Switzerland) [32], the sample was loaded in a silica capillary and cooled to 6 K using a side-loading cryostat. Powder diffraction patterns were collected in the temperature range between 6 and 25 K using an x-ray energy of 22 keV ($\lambda = 0.5635$ Å) and a wide-angle detector spanning $2\theta = 2°$–$85°$. The patterns were refined using the TOPAS package [33]. Additional high-resolution neutron diffraction was carried out using the HRPT instrument at the SINQ neutron source, also at PSI [34]. The neutron diffraction patterns for wavelengths 1.494 and 1.886 Å were corefined using the FULLPROF suite [35]. Inelastic neutron scattering was performed on the IN4C time-of-flight spectrometer at Institut Laue-Langevin using an incident energy $E_i = 16.9$ meV—the data are the same as that reported in Ref. [25]. Density functional calculations were performed using the full potential local orbital (FPLO) basis [36] and generalized gradient approximation (GGA) exchange correlation functional [37]. The strong electronic correlations of the $3d$ orbitals of Cr^{3+} were accounted for using a GGA + U correction [38].

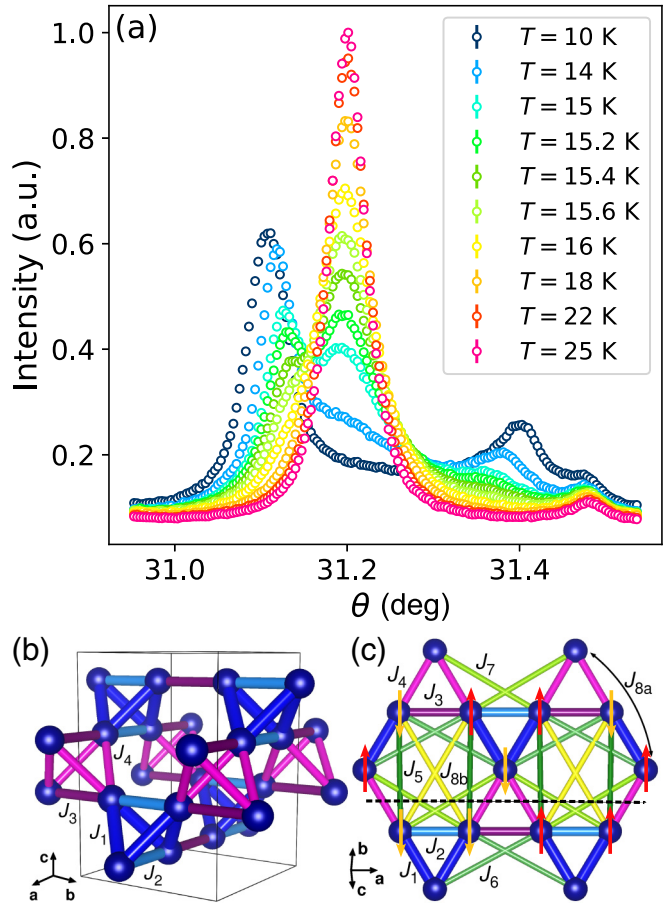

FIG. 1. (a) Temperature dependence of the (800) cubic peak in synchrotron x-ray powder diffraction data. At 16 K, two side peaks are observed, indexed as (008) and (440) in the tetragonal basis. These grow and shift on cooling, with the intensity of the cubic peak conversely reducing, until $T_l \simeq 13$ K is reached, below which they stop evolving. The tetragonal phase fraction is around 70% at low temperature. (b), (c) The low-temperature tetragonal $I\bar{4}m2$ structure. The colored bonds between the atoms indicate the four inequivalent Cr-Cr bonds corresponding to $J_{1\text{–}4}$. Further-neighbor couplings are shown in (c). The colored arrows schematically represent the magnetic order (the actual moment direction is $||c$). Note that J_4 remains frustrated in the ordered state, and that the only further-neighbor coupling up to J_8 that is not frustrated is the weak ferromagnetic J_6 (see Fig. 2). This effectively decouples the structure into planes of small tetrahedra denoted by the dashed line.

We begin by discussing the low-temperature atomic structure of $LiInCr_4O_8$, which was not fully determined in a previous study [25]: Its onset is indicated in our powder synchrotron x-ray diffraction data by the appearance of two side peaks near the cubic (008) diffraction peak at $T = 16$ K $\sim T_u$ [Fig. 1(a)]. This splitting implies that the low-temperature phase is of tetragonal or lower symmetry. At the same time, the absence of splitting in the (111) peak means that it is at least orthorhombic (within experimental resolution). The lattice parameters and phase fraction of the low-temperature phase evolve smoothly until T_u is reached, at which point the magnetic diffraction peaks (not shown) appear at small angles in the neutron diffraction data, and both the phase fraction

TABLE I. Structural parameters of the $I\bar{4}m2$ model refined from synchrotron x-ray powder diffraction data collected with $\lambda = 0.5635$ Å at 2 K at MS-X04A beamline at SLS, PSI. Lattice parameters: $a = 5.9480(2)$ Å, $c = 8.3380(3)$ Å. Refinement agreement factor $R_{wp} = 9.04$.

Atom	x	y	z	Wyck.
^{7}Li	0.00000	0.00000	0.00000	2*a*
In	0.00000	0.50000	0.75000	2*d*
Cr	0.00000	0.7437(2)	0.3699(2)	8*i*
O1	0.00000	0.2779(9)	0.1340(6)	8*i*
O2	0.00000	0.2222(8)	0.6079(6)	8*i*

and lattice parameter become nearly temperature independent. The inhomogeneity of the sample is likely due to variations in the local Li stoichiometry, which suppress the selection of a unique magnetostructural ground state. The peak profile of both phases shows significant broadening at all temperatures, previously ascribed to the combined effect of spin-lattice coupling-induced strain in the high-temperature structure and finite-size domains in the low-temperature structure [25].

Refining the 6-K x-ray diffraction data to a series of models that contain the high-temperature $F\bar{4}3m$ structure and each of its maximal subgroups, the best fit for the low-temperature structure is found for the tetragonal $I\bar{4}m2$ subgroup. Lowering the symmetry further leads to little improvement in χ^2, despite the crystal system of the previously determined magnetic structure being orthorhombic. This indicates that any orthorhombic distortion induced by the magnetic structure is slight. The refined parameters are shown in Table I. All are in good agreement with refinements of the neutron diffraction data at 2 K to the same model, and the refined phase fractions indicate that around 70% of the sample is in the low-temperature $I\bar{4}m2$ structure below T_l. In this structure, the c axis is compressed by around 0.6% and expanded along a by 0.3%, with the result that the small tetrahedra contain four short and two long bonds, while the large tetrahedra contain two short and four long bonds. The corresponding Cr-Cr bond distances are 2.900(4) and 2.865(3) Å (along $\langle 110\rangle$ and $\langle 011\rangle/\langle 101\rangle$, respectively) in the small tetrahedra, versus 2.880 Å in the undistorted structure, and 3.048(4) and 3.057(3) Å for the large tetrahedra, similar to 3.050 Å in the undistorted structure.

The previously determined magnetic structure of $LiInCr_4O_8$ is a nearly collinear antiferromagnetic arrangement with two spins up and two down on each tetrahedron, as predicted by Monte Carlo simulations of the site-phonon model on the breathing pyrochlore lattice [29]. Due to geometric frustration, only four bonds on a tetrahedron can be satisfied simultaneously for such an arrangement, assuming all of the exchanges are antiferromagnetic. Introducing the spin-lattice coupling, some of the frustration may be relieved by shortening the antiferromagnetic bonds and lengthening the ferromagnetic ones. On the small tetrahedra, the ferromagnetically coupled spins indeed lie along the long bonds (corresponding to J_2) and the antiferromagnetic ones along the short bonds (J_1). On the large tetrahedra, however, two of the long bonds (J_4) are ferromagnetic and two antiferromagnetic, while the two short bonds (J_3) are antiferromagnetic, as expected. This means that the total exchange energy for the long bonds is zero, and that no energy is gained by distorting the tetrahedron assuming that the magnitude of the exchange is simply related to the nearest-neighbor Cr-Cr distances, as in the bond-phonon model (the site-phonon model generates additional further-neighbor interactions [29]). This scenario is consistent with the minimal change in bond length between the low- and high-temperature structures, and indicates that it is the distortion of the small tetrahedra that gains the magnetoelastic energy that drives the transition. Furthermore, since the breathing pyrochlore lattice can be described as a stack of alternating small and large tetrahedra, the consequence of the net zero exchange energy over the long bonds in the latter is that spins on adjacent layers of small tetrahedra can be flipped without changing the total energy. Indeed, this effective dimensional reduction may be the origin of the broad magnetic diffraction peaks (correlation length $\xi = 44$ Å) observed in earlier polarized neutron diffraction [25], and indicates that some of the degeneracy associated with the frustration may remain in the low-temperature structure. Should single crystals become available, these short-range correlations should manifest as rods of diffuse scattering along the $(00l)$-type directions. Having established that the $I\bar{4}m2$ atomic model and its associated magnetic order are a good approximation to the low-temperature structure of $LiInCr_4O_8$, we now turn to its low-temperature magnetic Hamiltonian. We first determine the Heisenberg exchange interactions of $LiInCr_4O_8$ using density functional theory-based energy mapping. This approach is very successful in elucidating the relevant Hamiltonian both for quantum [39] and classical spin systems [40], and it had provided insight into several chromium spinels [41,42]. We use the same approach for the body-centered-tetragonal structure of $LiInCr_4O_8$ that was applied to the cubic high-temperature structure [16]. From this earlier study, we know that it is most important to determine the four nearest-neighbor interactions $J_{1\text{–}4}$ that replace the J, J' model; further-neighbor couplings were found to be very small in the case of breathing chromium spinel oxides [16]. The energy mapping was performed using the synchrotron x-ray powder diffraction (SXRPD) structure given in Table I in a fivefold supercell with $P1$ space group, allowing for spin configurations with 20 symmetry-inequivalent Cr sites (for more details, see the Supplemental Material [43]). The result is shown in Fig. 2, with the vertical line indicating the U value at which the Hamiltonian parameters yield the experimental Curie-Weiss temperature $\theta_{\mathrm{CW}} = -332$ K [11].

The resulting Hamiltonian has a substantial difference between J_1 and J_2 (originally J), with $J_2 = 0.46J_1$, and between J_3 and J_4 (originally J'), with $J_4 = 0.37J_3$. An important consequence is that the originally fully three-dimensional magnetic Hamiltonian becomes nearly two dimensional, with only the weakest nearest-neighbor coupling J_4 connecting the bilayers defined by small (J_1-J_2) tetrahedra and J_3 along the c direction. While the "second-neighbor" couplings J_5 to J_7 are quite small, the "third-neighbor" couplings $J_{8a} = 0.04J_1$ and $J_{8b} = 0.03J_1$ are nonzero. However, both of these are

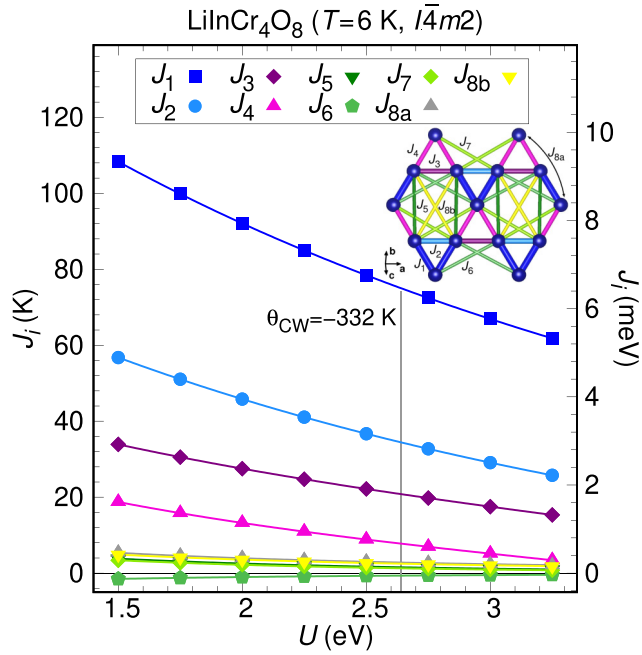

FIG. 2. The magnitude of the exchange couplings J_i described in the text vs the on-site repulsion U for nearest- and next-nearest-neighbor Cr-Cr bonds. The values corresponding to the experimental Curie-Weiss temperature $\theta_{\rm CW}$ are marked by a vertical line.

unable to relieve the degeneracy associated with the dimensional reduction [see Fig. 1(c)]. Indeed, it is only the weak ferromagnetic J_6 that is unfrustrated in the observed magnetic structure, Fig. 1(c). This means that the magnetic order must be due to other (effective) long-range interactions or terms beyond the Heisenberg model.

We next compare the predictions of our DFT model with inelastic neutron scattering experiments [25]. The dynamic structure factor $S(Q, \hbar\omega)$ measured at 1.7 K is shown in Fig. 3(a). The spectrum is dominated by a mode dispersing from $|Q| \simeq 1.75$ Å^{-1}, in the vicinity of the $(\frac{1}{2}\frac{1}{2}1)$ peak (in the tetragonal basis) of the low-temperature magnetic structure. There are also intensity maxima at around 6 and 8 meV, and the overall bandwidth of the magnetic excitations is around 13 meV. As a first attempt to model the experimental spectrum, we calculate the powder-averaged linear spin-wave spectrum for the $U = 2.66$ eV parameters using the SPINW package [44]. Only the nearest-neighbor exchanges were considered due to the very small magnitude of $J_{5\text{–}8}$. To compare with experiment, the simulated $S(|Q|, \hbar\omega)$ was convolved with the instrumental resolution and an additional broadening along ΔE and $|Q|$ due to the finite size of the magnetic domains. As can be seen in Fig. 3(c), the magnetic structure and many of the features of the experimental spectrum are correctly predicted, although the overall bandwidth is larger in the simulation than experiment. We note that the decoupling of the bilayers discussed above

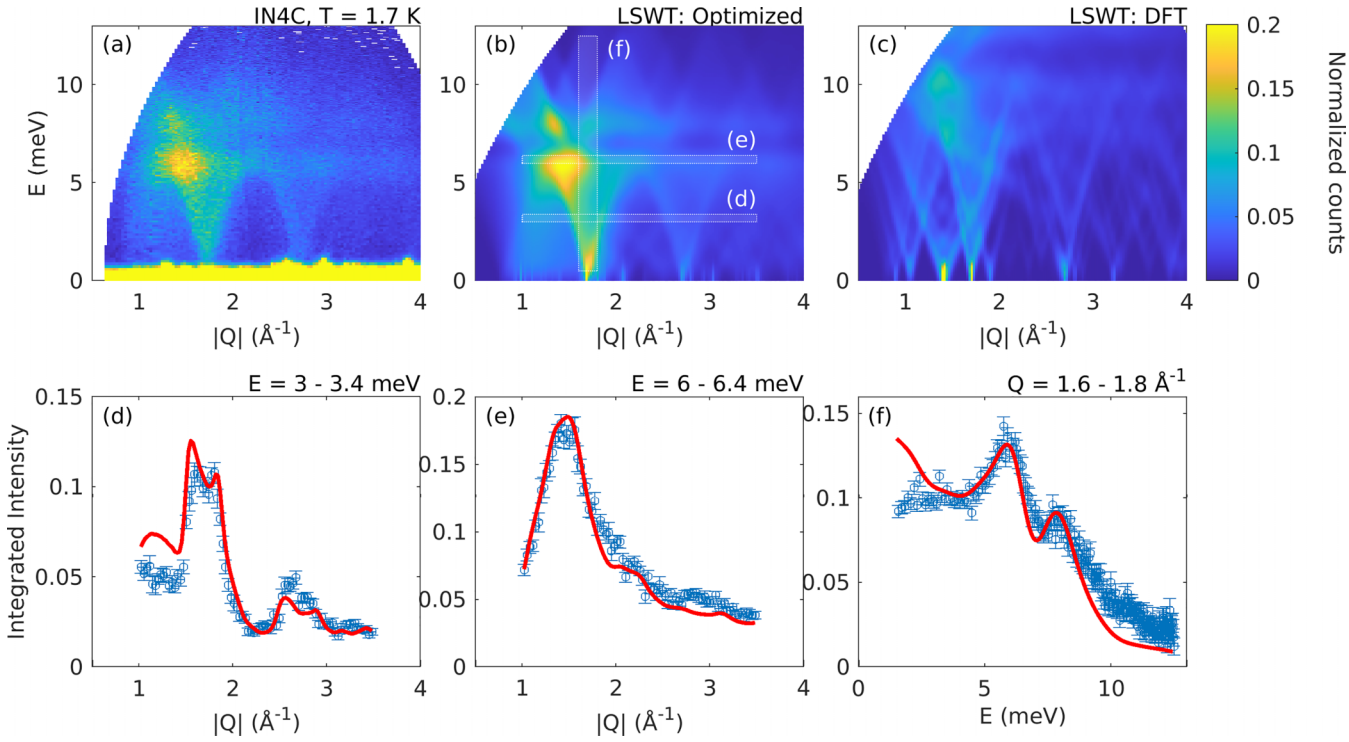

FIG. 3. (a) The experimental $S(|Q|, E = \hbar\omega)$ measured at 1.7 K on the IN4C spectrometer with an incident neutron energy $E_i = 16.9$ meV. (b) Spin-wave spectrum calculated from linear spin-wave theory using $J_1 = 74.52$ K (6.42 meV), $J_2 = 52.72$ K (4.54 meV), $J_3 = 12.35$ K (1.06 meV), and $J_4 = 6.81$ K (0.59 meV). The shaded boxes represent the integration ranges for the cuts displayed in (d)–(f). (c) Spectrum calculated from DFT parameters at $U = 2.66$ eV. (d)–(f) Cuts through the experimental data (blue circles) showing the fits to the optimized model.

is observed as a flat zero-energy mode along [001] in **Q**-resolved simulated spectra (see Supplemental Material [43] Fig. S5).

Given the good qualitative agreement between the experimental spectrum and that generated from the DFT calculations, we proceed to optimize the exchange parameters as follows: First, five diagnostic constant-$|Q|$ cuts through the data were selected for the calculation of $\chi^2 = [S(|Q|, E)_{\text{obs}} - S(|Q|, E)_{\text{calc}}]^2$. Then, χ^2 was evaluated for a $10\times10\times10\times10$ grid in the parameters $J_{1\text{–}4}$. The grid was restricted to a volume of parameter space consistent with the magnetic structure by requiring that $J_1 > J_2$ and $J_3 > J_4$. Finally, a local minimization was carried out in the vicinity of the lowest 16 points identified in the grid search [43]. This procedure revealed several solutions with J_1 ranging from ∼3.8 to 8.6 meV. Despite the large parameter range, all of the solutions are constrained by the relation $(J_1 + J_4)/(J_2 + J_3) \simeq 1.24$. The nearly identical χ^2 from these is due to the fact that $J_{1(2)}$ and $J_{4(3)}$ correspond to bonds that lie along the same direction, and therefore contribute nearly identical Fourier components to $J(\mathbf{Q})$. The physical meaning of the value 1.24 becomes clearer on rewriting the exchanges on the small and large tetrahedra in terms of deviations from an average exchange J_a, J'_a (note that these are not necessarily the high temperature J, J'): $J_1 = J_a + \delta$, $J_2 = J_a - \delta$, $J_3 = J'_a + \delta'$, $J_4 = J'_a - \delta'$. For the ratio in terms of this new parametrization to exceed 1, it is necessary for $\delta > \delta'$ and for $(J_a - \delta + J'_a + \delta') > 0$. If J_a, J'_a are assumed to be close to high-temperature J, J', and associating larger δ with larger distortions, the former is consistent with the low-temperature crystal structure, and points to the gain in magnetic energy represented by δ driving the transition; the energy per pair of tetrahedra in the low-temperature state versus the undistorted state is $-(6\delta + 2\delta')S^2$. Comparing the fitted and DFT parameters shows that the parameter ratios are broadly consistent [43]—while the agreement is best for small U, work on related materials and the high-temperature Weiss constant θ_{CW} suggests a larger value.

The $S(|Q|, \Delta E)$ and cuts for the parameters above are shown in Figs. 3(b) and 3(d)–3(f); the overall agreement between the data and model is almost quantitative. This is particularly surprising because it implies that the spectral weight corresponding to the minority cubic phase at low temperature is negligible. The disagreement between calculation and experiment is most pronounced at small and large energies, where the experimental intensity is lower and higher than the calculated one, respectively. The former observation can be explained by the short correlation length in the low-temperature state suppressing magnons with wavelengths that exceed it. We finally note that besides the further-neighbor couplings, both the Dzyaloshinskii-Moriya and spin-lattice coupling are omitted in our model: The former is likely to be present due to the fact that the magnetic structure is actually incommensurate (as in $CdCr_2O_4$ [45]), and may be the term that stabilizes the observed magnetic order. As for the latter, assuming that it can be approximated by the leading biquadratic term in the site-phonon model and given that the magnetic structure is close to collinear, its effect should only be to renormalize the magnitude of the bilinear exchanges [46].

To conclude, we have presented a comprehensive study of the low-temperature magnetic and atomic structure of the breathing pyrochlore system $LiInCr_4O_8$ using neutron and synchrotron x-ray diffraction, inelastic neutron scattering, and density functional theory. The atomic structure is well approximated by a tetragonal $I\bar{4}m2$ model where the small and large tetrahedra have two long and four short bonds, and four long and two short bonds, respectively. The pattern of distortions on the small tetrahedra is consistent with the magnetic structure assuming that the spin-lattice coupling drives the lifting of geometric frustration. The large tetrahedra, however, remain nearly undistorted due to the persistence of frustration along one of the distortion axes. This leads to a decoupling of the lattice between adjacent planes of small tetrahedra, which could explain the finite correlation length of the magnetic peaks in previous diffraction experiments. DFT calculations based on the new low-temperature crystal structure demonstrate that there is a large modulation of the exchanges due to the structural distortion, with the weakest nearest-neighbor exchange on the large tetrahedra being around an order of magnitude smaller than the leading exchange in the small tetrahedra. In addition, further-neighbor couplings are found to be <5% of J_1. The DFT exchange parameters were used to simulate the linear spin wave $S(|Q|, E)$, which was compared to the magnetic excitation spectrum measured by inelastic spectroscopy. Many of the features of the latter are captured by the simulation, and further optimization of $J_{1\text{–}4}$ leads to an almost quantitative agreement for several parameter sets that obey the relation $(J_1 + J_4)/(J_2 + J_3) \simeq 1.24$. Distinguishing between these parameter sets will require additional experiments; the most straightforward way would be to measure the critical field, which should be proportional to the sum of the exchange constants. This is likely to require fields in excess of 500 T, however. This deficiency notwithstanding, the dynamics in the low-temperature phase of a Cr^{3+} spinel have been successfully modeled.

We are grateful to M. Duc Le (ISIS) for many useful discussions regarding fitting to inelastic neutron data from powder data. We thank the ILL for beamtime on the IN4 spectrometer. G.J.N. thanks Tohoku University for hosting under GIMRT Proposals No. 202212-CNKXX-0504 and No. 202312-CNKXX-0502. Y.O. acknowledges support from JST-ASPIRE, No. JPMJAP2314.

The data that support the findings of this article are openly available [47].

[1] O. A. Starykh, Unusual ordered phases of highly frustrated magnets: A review, Rep. Prog. Phys. **78**, 052502 (2015).

[2] H. Shinaoka, Y. Tomita, and Y. Motome, Effect of magnetoelastic coupling on spin-glass behavior in Heisenberg pyrochlore antiferromagnets with bond disorder, Phys. Rev. B **90**, 165119 (2014).

[3] O. Benton and N. Shannon, Ground-state selection and spin-liquid behaviour in the classical Heisenberg model on the

breathing pyrochlore lattice, J. Phys. Soc. Jpn. **84**, 104710 (2015).
[4] G.-W. Chern, R. Moessner, and O. Tchernyshyov, Partial order from disorder in a classical pyrochlore antiferromagnet, Phys. Rev. B **78**, 144418 (2008).
[5] S.-H. Lee, C. Broholm, T. H. Kim, W. Ratcliff, and S.-W. Cheong, Local spin resonance and spin-Peierls-like phase transition in a geometrically frustrated antiferromagnet, Phys. Rev. Lett. **84**, 3718 (2000).
[6] O. Tchernyshyov, R. Moessner, and S. L. Sondhi, Spin-Peierls phases in pyrochlore antiferromagnets, Phys. Rev. B **66**, 064403 (2002).
[7] N. Shannon, K. Penc, and Y. Motome, Nematic, vector-multipole, and plateau-liquid states in the classical $O(3)$ pyrochlore antiferromagnet with biquadratic interactions in applied magnetic field, Phys. Rev. B **81**, 184409 (2010).
[8] A. Miyata, H. Ueda, Y. Ueda, Y. Motome, N. Shannon, K. Penc, and S. Takeyama, Novel magnetic phases revealed by ultra-high magnetic field in the frustrated magnet $ZnCr_2O_4$, J. Phys. Soc. Jpn. **80**, 074709 (2011).
[9] S. Ji, S.-H. Lee, C. Broholm, T. Y. Koo, W. Ratcliff, S.-W. Cheong, and P. Zschack, Spin-lattice order in frustrated $ZnCr_2O_4$, Phys. Rev. Lett. **103**, 037201 (2009).
[10] We note that the nature of this magnetostructural order remains controversial.
[11] Y. Okamoto, G. J. Nilsen, J. P. Attfield, and Z. Hiroi, Breathing pyrochlore lattice realized in *A*-site ordered spinel oxides $LiGaCr_4O_8$ and $LiInCr_4O_8$, Phys. Rev. Lett. **110**, 097203 (2013).
[12] Y. Okamoto, G. J. Nilsen, T. Nakazano, and Z. Hiroi, Magnetic phase diagram of the breathing pyrochlore antiferromagnet $LiGa_{1-x}In_xCr_4O_8$, J. Phys. Soc. Jpn. **84**, 043707 (2015).
[13] Y. Okamoto, M. Mori, N. Katayama, A. Miyake, M. Tokunaga, A. Matsuo, K. Kindo, and K. Takenaka, Magnetic and structural properties of A-site ordered chromium spinel sulfides: Alternating antiferromagnetic and ferromagnetic interactions in the breathing pyrochlore lattice, J. Phys. Soc. Jpn. **87**, 034709 (2018).
[14] R. Plumier and M. Sougi, Mise en evidence par diffraction des neutrons d'un terme d'echance biquadratique dans l'helimagnetique $Ag_{1/2}In_{1/2}Cr_2S_4$, Solid State Commun. **9**, 413 (1971).
[15] R. Plumier, F. K. Lotgering, and R. P. van Stapele, Magnetic properties of $Cu_{1/2}In_{1/2}Cr_2S_4$ and some related compounds, J. Phys. Colloq. **32**, C1 (1971).
[16] P. Ghosh, Y. Iqbal, T. Müller, R. T. Ponnaganti, R. Thomale, R. Narayanan, J. Reuther, M. J. P. Gingras, and H. O. Jeschke, Breathing chromium spinels: A showcase for a variety of pyrochlore Heisenberg Hamiltonians, npj Quantum Mater. **4**, 63 (2019).
[17] G. Pokharel, H. S. Arachchige, T. J. Williams, A. F. May, R. S. Fishman, G. Sala, S. Calder, G. Ehlers, D. S. Parker, T. Hong, A. Wildes, D. Mandrus, J. A. M. Paddison, and A. D. Christianson, Cluster frustration in the breathing pyrochlore magnet $LiGaCr_4S_8$, Phys. Rev. Lett. **125**, 167201 (2020).
[18] D. Reig-i-Plessis and A. M. Hallas, Frustrated magnetism in fluoride and chalcogenide pyrochlore lattice materials, Phys. Rev. Mater. **5**, 030301 (2021).
[19] S. Gao, A. F. May, M.-H. Du, J. A. M. Paddison, H. S. Arachchige, G. Pokharel, C. dela Cruz, Q. Zhang, G. Ehlers, D. S. Parker, D. G. Mandrus, M. B. Stone, and A. D. Christianson, Hierarchical excitations from correlated spin tetrahedra on the breathing pyrochlore lattice, Phys. Rev. B **103**, 214418 (2021).
[20] A. Szabó and G. J. Nilsen, Dynamics of the antiferromagnetic spin ice phase in pyrochlore spinels, Phys. Rev. B **109**, 104425 (2024).
[21] S. Gao, Dynamic spin-lattice coupling and statistical interpretation for the molecularlike excitations in frustrated pyrochlores, Phys. Rev. B **110**, 214420 (2024).
[22] F.-Y. Li, Y.-D. Li, Y. B. Kim, L. Balents, Y. Yu, and G. Chen, Weyl magnons in breathing pyrochlore antiferromagnets, Nat. Commun. **7**, 12691 (2016).
[23] L. E. Chern, Y. B. Kim, and C. Castelnovo, Competing quantum spin liquids, gauge fluctuations, and anisotropic interactions in a breathing pyrochlore lattice, Phys. Rev. B **106**, 134402 (2022).
[24] R. Saha, F. Fauth, M. Avdeev, P. Kayser, B. J. Kennedy, and A. Sundaresan, Magnetodielectric effects in *A*-site cation-ordered chromate spinels $LiMCr_4O_8$ (M = Ga and In), Phys. Rev. B **94**, 064420 (2016).
[25] G. J. Nilsen, Y. Okamoto, T. Masuda, J. Rodriguez-Carvajal, H. Mutka, T. Hansen, and Z. Hiroi, Complex magnetostructural order in the frustrated spinel $LiInCr_4O_8$, Phys. Rev. B **91**, 174435 (2015).
[26] S. Lee, S.-H. Do, W.-J. Lee, Y. S. Choi, M. Lee, E. S. Choi, A. P. Reyes, P. L. Kuhns, A. Ozarowski, and K.-Y. Choi, Multistage symmetry breaking in the breathing pyrochlore lattice $Li(Ga, In)Cr_4O_8$, Phys. Rev. B **93**, 174402 (2016).
[27] Z. He, Y. Gu, H. Wo, Y. Feng, D. Hu, Y. Hao, Y. Gu, H. C. Walker, D. T. Adroja, and J. Zhao, Neutron scattering studies of the breathing pyrochlore antiferromagnet $LiGaCr_4O_8$, Phys. Rev. Lett. **127**, 147205 (2021).
[28] M. Gen, D. Nakamura, Y. Okamoto, and S. Takeyama, Ultrahigh magnetic field magnetic phases up to 130 T in a breathing pyrochlore antiferromagnet $LiInCr_4O_8$, J. Magn. Magn. Mater. **473**, 387 (2019).
[29] K. Aoyama and H. Kawamura, Spin ordering induced by lattice distortions in classical Heisenberg antiferromagnets on the breathing pyrochlore lattice, Phys. Rev. B **99**, 144406 (2019).
[30] K. Aoyama, M. Gen, and H. Kawamura, Effects of spin-lattice coupling and a magnetic field in classical Heisenberg antiferromagnets on the breathing pyrochlore lattice, Phys. Rev. B **104**, 184411 (2021).
[31] Y. Okamoto, D. Nakamura, A. Miyake, S. Takeyama, M. Tokunaga, A. Matsuo, K. Kindo, and Z. Hiroi, Magnetic transitions under ultrahigh magnetic fields of up to 130 T in the breathing pyrochlore antiferromagnet $LiInCr_4O_8$, Phys. Rev. B **95**, 134438 (2017).
[32] P. R. Willmott, D. Meister, S. J. Leake, M. Lange, A. Bergamaschi, M. Böge, M. Calvi, C. Cancellieri, N. Casati, A. Cervellino, Q. Chen, C. David, U. Flechsig, F. Gozzo, B. Henrich, S. Jäggi-Spielmann, B. Jakob, I. Kalichava, P. Karvinen, J. Krempasky *et al.*, The materials science beamline upgrade at the Swiss light source, J. Synchrotron Radiat. **20**, 667 (2013).
[33] A. Coelho, Coelho Software, TOPAS-Academic v5 (2012), http://www.topas-academic.net/.

[34] P. Fischer, G. Frey, M. Koch, M. Könnecke, V. Pomjakushin, J. Schefer, R. Thut, N. Schlumpf, R. Bürge, U. Greuter, S. Bondt, and E. Berruyer, High-resolution powder diffractometer HRPT for thermal neutrons at SINQ, Phys. B: Condens. Matter **276-278**, 146 (2000).

[35] J. Rodriguez-Carvajal, Recent advances in magnetic structure determination by neutron powder diffraction, Phys. B: Condens. Matter **192**, 55 (1993).

[36] K. Koepernik and H. Eschrig, Full-potential nonorthogonal local-orbital minimum-basis band-structure scheme, Phys. Rev. B **59**, 1743 (1999).

[37] J. P. Perdew, K. Burke, and M. Ernzerhof, Generalized gradient approximation made simple, Phys. Rev. Lett. **77**, 3865 (1996).

[38] A. I. Liechtenstein, V. I. Anisimov, and J. Zaanen, Density-functional theory and strong interactions: Orbital ordering in Mott-Hubbard insulators, Phys. Rev. B **52**, R5467 (1995).

[39] I. Živković, V. Favre, C. S. Mejia, H. O. Jeschke, A. Magrez, B. Dabholkar, V. Noculak, R. S. Freitas, M. Jeong, N. G. Hegde, L. Testa, P. Babkevich, Y. Su, P. Manuel, H. Luetkens, C. Baines, P. J. Baker, J. Wosnitza, O. Zaharko, Y. Iqbal *et al.*, Magnetic field induced quantum spin liquid in the two coupled trillium lattices of $K_2Ni_2(SO_4)_3$, Phys. Rev. Lett. **127**, 157204 (2021).

[40] Y. Iqbal, T. Müller, H. O. Jeschke, R. Thomale, and J. Reuther, Stability of the spiral spin liquid in $MnSc_2S_4$, Phys. Rev. B **98**, 064427 (2018).

[41] M. Gen, A. Ikeda, K. Aoyama, H. O. Jeschke, Y. Ishii, H. Ishikawa, T. Yajima, Y. Okamoto, X. Zhou, D. Nakamura, S. Takeyama, K. Kindo, Y. H. Matsuda, and Y. Kohama, Signatures of a magnetic superstructure phase induced by ultrahigh magnetic fields in a breathing pyrochlore antiferromagnet, Proc. Natl. Acad. Sci. USA **120**, e2302756120 (2023).

[42] L. D. C. Jaubert, Y. Iqbal, and H. O. Jeschke, Spin-Peierls transition in the frustrated spinels $ZnCr_2O_4$ and $MgCr_2O_4$, Phys. Rev. Lett. **134**, 086702 (2025).

[43] See Supplemental Material at http://link.aps.org/supplemental/10.1103/wjh8-qt1x for additional information on the x-ray powder diffraction, density functional theory results, and the spin-wave fitting, which also includes Ref. [48].

[44] S. Toth and B. Lake, Linear spin wave theory for single-Q incommensurate magnetic structures, J. Phys.: Condens. Matter **27**, 166002 (2015).

[45] J.-H. Chung, M. Matsuda, S.-H. Lee, K. Kakurai, H. Ueda, T. J. Sato, H. Takagi, K.-P. Hong, and S. Park, Statics and dynamics of incommensurate spin order in a geometrically frustrated antiferromagnet $CdCr_2O_4$, Phys. Rev. Lett. **95**, 247204 (2005).

[46] A. L. Wysocki, K. D. Belashchenko, and V. P. Antropov, Consistent model of magnetism in ferropnictides, Nat. Phys. **7**, 485 (2011).

[47] G. Nilsen, T. C. Hansen, Z. Hiroi, T. Masuda, H. Mutka, Y. Okamoto, and C. Tassel, Magnetostructural coupling and spin dynamics in the 'breathing' pyrochlore antiferromagnets $LiInCr_4O_8$ and $LiGaCr_4O_8$ (2013), https://doi.org/doi:10.5291/ILL-DATA.5-31-2275.

[48] T. Mizokawa and A. Fujimori, Electronic structure and orbital ordering in perovskite-type 3d transition-metal oxides studied by Hartree-Fock band-structure calculations, Phys. Rev. B **54**, 5368 (1996).